Biochar X

Original Research

Open Access

https://doi.org/10.48130/bchax-0025-0004

Investigation of the CO_2 adsorption behavior of alkali-modified biochar components in cement composites

Binglin Guo[1,2,3*], Ping Ye[1], Huyong Qin[1], Cheng Wang[1], Yang Liu[1], Yuyang Chen[1], Pengfei Bian[1], Di Lu[1], Lei Wang[4*], Tongsheng Zhang[5*], Weiping Zhao[1], Binggen Zhan[1,2,3] and Qijun Yu[2,3,5]

Received: 14 July 2025

Revised: 16 August 2025

Accepted: 10 September 2025

Published online: 20 October 2025

Abstract

Incorporating biochar into cement offers an effective strategy to reduce carbon emissions. However, the structural heterogeneity of the original biochar limits its capacity for CO_2 adsorption. In this work, biochar was produced by pyrolyzing corn straw at 300, 500, and 700 °C, and its main heterogeneous component—sedimented particles (SP)—was obtained through physical separation. Subsequently, both the original biochar and SP were treated with alkali to investigate their CO_2 adsorption capacities. Furthermore, original biochar, SP, CO_2-saturated modified biochar, and CO_2-saturated modified SP were each incorporated into cement composites at dosages of 1%, 2%, 3%, and 5% by cement mass to evaluate their effects on the mechanical properties and carbon sequestration performance. The results demonstrated that SP had a higher CO_2 adsorption capacity than the original biochar, and this capacity increased further with rising pyrolysis temperature. The adsorption kinetics indicate that biochar primarily undergoes physical adsorption of CO_2, with a minor contribution from chemical adsorption. Furthermore, as the pyrolysis temperature of biochar increased, its effects on cement composites led to a trend of first increasing and then decreasing hydration product formation. The CO_2-saturated modified SP resulted in higher compressive strength compared to cement composites containing SP alone at a substitution rate of 1%. This work provides insights that promote the effective utilization of biochar in the carbon sequestration of cement composites.

Keywords: Biochar, CO_2 adsorption, Alkali-modified, Carbon sequestration, Cement composites

Highlights

- The CO_2 adsorption of the sedimented particles surpasses that of the original biochar.
- Biochar pyrolyzed at 500 °C has the best CO_2 adsorption capacity.
- Alkali modification improves the microporous structure of biochar.
- CO_2-adsorbed modified biochar further enhances the compressive strength of cement composites.

* Correspondence: Binglin Guo (gabriel116329@hotmail.com); Lei Wang (wanglei.leo@zju.edu.cn); Tongsheng Zhang (mstszhang@scut.edu.cn)
Full list of author information is available at the end of the article.

Graphical abstract

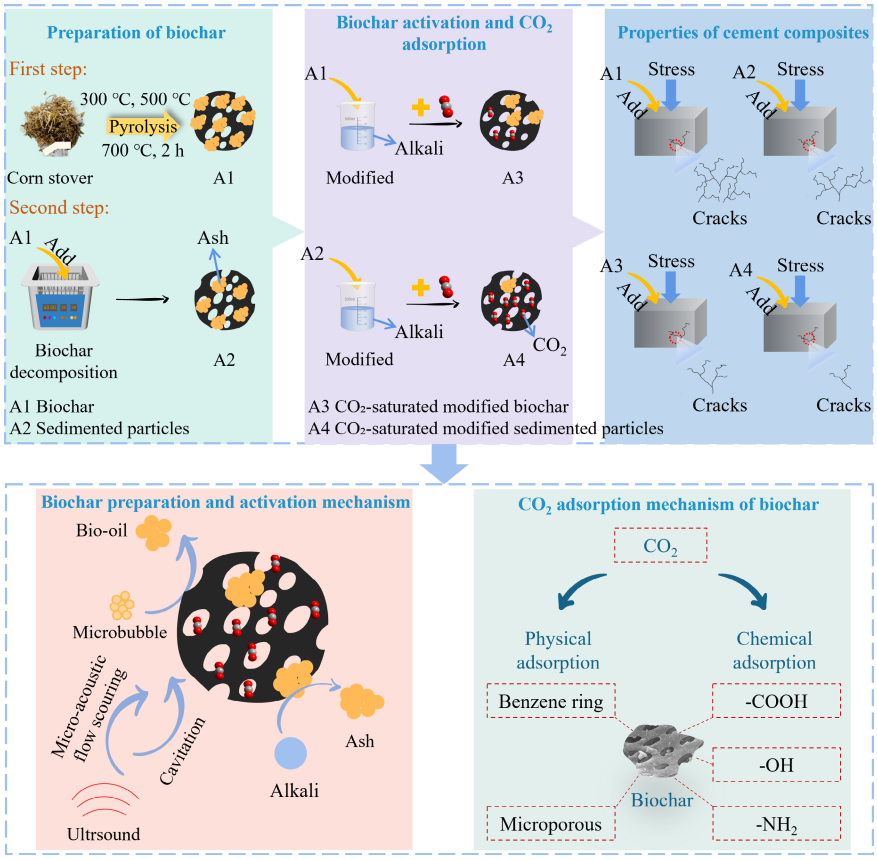

Introduction

In recent years, cement, as the most extensively utilized construction material globally, has contributed to a variety of environmental problems—such as global warming, air pollution, and sea level rise—due to its high CO_2 emissions, thereby posing a serious threat to human survival and development[1]. Despite the decline in total cement output driven by macroeconomic factors, technological advancements, and market changes, the pressure to reduce carbon emissions remains severe[2,3]. Consequently, a range of technologies have been explored to effectively mitigate CO_2 emissions, including carbon sequestration and cleaner fuel use[4,5]. For instance, Wang et al. highlighted that the utilization of compressed natural gas reduces energy consumption, CO_2 emissions, and air pollutants compared to conventional fuels[6]. Afari et al. discovered that a moderate addition of ethanolamine (MEA) to methyl diethanolamine (MDEA) solution significantly increases the rate of CO_2 absorption[7]. Although numerous techniques demonstrate promising CO_2 capture capabilities, their large-scale application in the cement industry remains constrained by high costs and limited efficiency. In response, carbon capture and storage (CCS) has gained increasing attention for its low cost, high efficiency, ability to limit the production of harmful by-products, and wide range of applications. Among the various CCS materials, biochar is considered a promising material for its high specific surface area (SSA), chemical stability, porous character, and reduced land demand for waste disposal[2,8].

Biochar is produced by pyrolyzing biomass into sustainable porous sequestered carbon materials under anaerobic conditions. Previous studies indicated that biochar's CO_2 uptake was mainly influenced by its microporous structure (van der Waals force-induced physical adsorption), and alkalinity (Lewis acid-base reaction-induced chemical adsorption)[9]. Thus, the adsorption performance of biochar mainly depends on its physicochemical properties, which are mainly influenced by the types of feedstock and pyrolysis conditions (e.g., temperature and pressure)[10]. Among them, pyrolysis temperature is considered to be a key factor in controlling the adsorption capacity of biochar at atmospheric pressure. For example, Li et al. pointed out that at pyrolysis temperatures of 600–800 °C, biochar produced from rice husks exhibited the highest CO_2 uptake at 700 °C[11]. Lahijani et al. discovered that pyrolysis-induced structural changes in biochar enhanced its adsorption capacity with increasing pyrolysis temperature[12]. Xu et al. pointed out that slow pyrolysis under high-temperature conditions favors the generation of a large SSA and well-developed pore structure of biochar, resulting in enhanced adsorption properties[3]. However, the uptake of the original biochar remains insufficient to meet the demand posed by anthropogenic CO_2 emissions. Therefore, numerous studies have been conducted to modify biochar via various modification approaches (e.g., physical, chemical, and biological) to improve its CO_2 uptake capacity. For instance, Ghanbari et al. highlighted that MgO impregnation enhances biochar's crystalline structure and improves the diffusion flux through the large pores, thus increasing its CO_2 adsorption capacity[13]. Zhu et al. reported that acid-modified biochar effectively removed a large number of soluble components, including metal salts and carbonates[14]. In contrast, alkali modification increases SSA and optimizes the pore architecture of biochar, thereby enhancing its CO_2 adsorption capacity[15].

With the advancement of biochar modification, the application of biochar with excellent physicochemical properties in the cement industry has attracted increasing attention[8,16]. For example, Zeidabadi et al. highlighted that adding a 1% dose of biochar to concrete can absorb 20% of the cement industry's total CO_2 emissions annually[17]. Wang et al. discovered that adding a 4% dose of biochar to concrete can sequester 0.124 kg of CO_2[2]. Gupta et al. pointed out that the incorporation of biochar with adsorbed CO_2 into cement composites reduces overall carbon emissions[18]. These results show that biochar is a promising material for CO_2 sequestration in the cement industry. Moreover, the incorporation of biochar not only enhances the carbon sequestration capacity but also improves the mechanical properties of cement composites. For instance, Javed et al. indicated that the incorporation of biochar into concrete resulted in a denser internal structure and higher compressive strength[19]. Choi et al. highlighted that replacing mortar with biochar produced from hardwoods at a 5% mixing ratio enhanced compressive strength by 10%. However, higher biochar substitution ratios (e.g., 10%, 15%, 20%) resulted in lower compressive strength[20]. With further research, scholars have investigated the impact of structural heterogeneity of biochar on the properties of cement composites. Specifically, during the biochar decomposition, soluble minerals dissolve, and surface particles gradually dissociate from the original biochar. As a result, decomposed biochar can be specifically classified as sedimented particles (SP), suspended coarse particles (CP), and soluble fractions along with ultrafine particles (SCUP)[21–25]. Compared with CP and SCUP, SP exhibits the most significant enhancement in the compressive strength of cement composites[26]. As the main component of biochar's heterogeneous structure, the SP possesses a superior SSA and pore structure, which results in enhanced CO_2 adsorption capacity compared to the other components. These results provide new insights for enhancing the CO_2 adsorption capacity of biochar by leveraging its heterogeneous structural features.

Despite the increasing attention on biochar cement composites, several challenges remain unresolved. Currently, most studies have studied the CO_2 adsorption effect of biochar as a whole component, while the CO_2 adsorption capacity of the heterogeneous structure of biochar remains underexplored. In addition, the use of CO_2-adsorbed SP in cement composites has not been investigated by experimental techniques. Therefore, the main objectives of this work are to: (i) Explore the impact of alkali modification on different components of biochar; (ii) Investigate the influence of different components of biochar on CO_2 adsorption performance; (iii) Analyze the effect of biochar on the properties of cement composites under various conditions, including different adsorption volumes of CO_2, pyrolysis temperatures, and addition ratios.

Materials and methods

Raw materials

The biochar (Shengxiang Activated Carbon Department, Gongyi City, China) used in this work was derived from corn stover and pyrolyzed at 300, 500, and 700 °C. The chemical components of biochar are listed in Table 1. For convenience, biochar samples are denoted as BC300, BC500, and BC700 according to their pyrolysis temperature. P.O. 42.5 ordinary Portland cement (OPC; Rongcai New Building Materials Co., Ltd., Anhui, China), and the composition and particle sizes of the substances detected are shown in Table 2 and Fig. 1, respectively. The results indicate that the median particle sizes of BC300, BC500, and BC700 are 10.9, 9.02, and 9 μm, respectively, which are smaller than the 15.14 μm size of OPC particles. Deionized water, produced by the Laboratory Ultrapure Water Distribution System (Lingde Instrument Co., Ltd., Shanghai, China), was used in this work. The chemical reagent sodium hydroxide (McLean Biochemicals Co., Ltd., Shanghai, China) was used in this work.

Table 1 Elemental distribution in biochar (wt.%)

Sample	C (%)	O (%)	Si (%)	Cl (%)	K (%)	Else (%)
BC300	35.70	25.14	13.19	1.26	5.73	18.98
SP300	38.50	19.39	11.67	–	1.67	28.77
BC500	40.63	33.35	17.71	0.94	3.55	3.82
SP500	44.59	20.06	18.19	–	4.13	13.03
BC700	43.05	6.58	21.17	0.87	8.83	19.50
SP700	45.58	19.10	21.88	–	2.78	10.66

Table 2 Chemical composition of OPC (wt.%)

Sample	CaO	SiO_2	Al_2O_3	CO_2	SO_3	Fe_2O_3	K_2O	Other
Content	44.64	25.13	11.57	8.36	3.45	3.35	1.11	2.39

Experimental methods

Specimen preparation

In this study, precipitated particles were prepared by the physical decomposition method[27]. Specifically, biochar (3 g) was dispersed in 100 mL of ultrapure water, dispersed for 30 min with an SK7200HP ultrasonic instrument (Shanghai Kedao Instrument and Equipment Co., Ltd, Shanghai, China), and then precipitated for 72 h. The precipitate in the beaker was collected as precipitated particles. Among them, the whole step was repeated twice. For the convenience of differentiation, the precipitated particles collected at 300, 500, and 700 °C above were denoted as SP300, SP500, and SP700, respectively.

The alkali-modified biochar was produced by dispersing 1 g of biochar in 40 mL of 1 mol·L^{-1} NaOH for 30 min, then modified, filtered, and dried. These samples were labeled as MBC300, MBC500, MBC700, MSP300, MSP500, and MSP700. Then, the different components of alkali-modified biochar were exposed to a nitrogen-filled environment in a rotary furnace, heated to 120 °C, and maintained for 1 h. After the furnace had cooled to room temperature, CO_2 was introduced for 2 h, after which the biochar was removed from the tube. These samples were denoted as CMBC300, CMBC500, CMBC700, CMSP300, CMSP500, and CMSP700. Among them, CMBC and CMSP represent CO_2-saturated modified biochar and CO_2-saturated modified SP, respectively. Previous studies have demonstrated that, as physical adsorption is the predominant mechanism

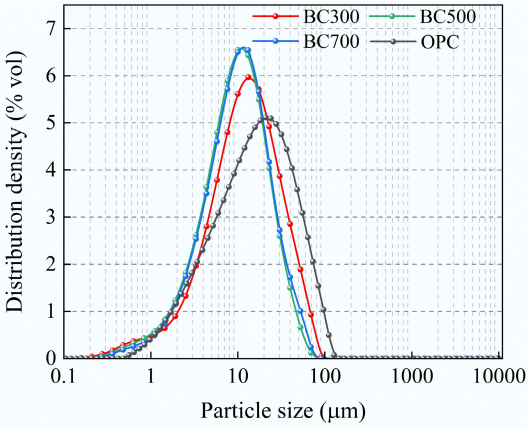

Fig. 1 Particle size distribution of BC300, BC500, BC700, and OPC.

of CO_2 capture by biochar, its morphology, physical properties, and chemical composition remain essentially unchanged after biochar pores are saturated with CO_2[17, 28,29]. This provides a useful reference for evaluating the effect of different alkali-modified biochar materials in cement composites.

The CO_2 adsorption experiments were conducted according to the procedures of previous studies[28]. Specifically, about 20 mg of biochar was introduced into an alumina crucible on the TGA, heated to 120 °C under a nitrogen atmosphere, and held for 1 h to remove biochar impurities (e.g., moisture and residual gases). Notably, the nitrogen flow rate for the impurity removal step matched that of the CO_2 flow rate for the adsorption step (50 mL·min^{-1}). Subsequently, when the temperature decreased to 25 °C, high-purity CO_2 was injected for mass measurement. The increase in sample mass represented the absorbed quantity of CO_2 (the amount of N_2 adsorbed on the sample is neglected). Blank tests were conducted under the same conditions. This baseline accounted for instrumentation and buoyancy effects to ensure correct mass change values[30].

This work explored the influence of biochar incorporated at levels of 1%, 2%, 3%, and 5% on the properties of cement composites. All samples were mixed with a water-to-cement ratio (w/c) of 0.4, and the experimental scheme is listed in Table 3 and Supplementary Table S1. The different materials were mixed homogeneously for 10 min in certain proportions and then moved to the cement mixer to experiment according to the automatic control program. Then, the mixture was poured into 4 cm × 4 cm × 4 cm molds, and maintained for 24 h before demolding. Finally, the samples were moved to standard conditions of (20 ± 1) °C and humidity above 90%, where they were maintained until the day of testing. Notably, three replicate samples were prepared for each test.

Characterization methods

The samples were cured for 7 and 28 d before the compressive strength test was conducted in accordance with the Chinese standard GB/T17671-2021[31]. The compressive strength average was calculated from the values of three specimens per group, and the standard deviation was indicated by error bars. After the strength experiments, fragments from all samples were collected and placed in anhydrous ethanol to halt hydration, and were then stored in a dry condition until the corresponding experiments. The samples were characterized using the following instruments:

A laser particle size analyzer (Mastersizer 2000, GBR) was employed to measure the particle size distribution of materials by measuring the scattered light intensity at various angles. A Brunauer-Emmett-Teller (Nova 4200E, USA, BET) was used to determine the SSA and pore volume of biochar. The nitrogen adsorption method (77.35K) was applied, with calculations based on the BET and Barrett-Joyner-Halenda (BJH) models. An X-ray fluorescence spectrometer (XRF-1800, JPN, XRF) was used to examine the elemental distribution in biochar and cement particles. X-ray diffraction (PANalytical X-Pert PRO MPD, NL, XRD) was used to analyze the compositional and structural information about the material at the atomic or molecular level. The test conditions included CuKα radiation, with a constant X-ray tube current of 40 mA and a voltage of 40 kV. Meanwhile, the scanning range was from 5 to 70° (2θ), with an increment of 0.02° and a step duration of 20 s. Fourier Transform Infrared Spectroscopy (Nexus 670, USA, FTIR) was employed to measure the absorption and reflection spectra of biochar within the infrared spectral region from 4,000 to 400 cm^{-1}, with a scan rate of 20 times per minute. Scanning Electron Microscope (Zeiss Sigma500 Field Emission, GER, SEM) was utilized to analyze the microscopic structure of different materials. Synchronous thermal analyzer (STA449F5, GER, TG) heated the sample from 20 to 800 °C at 10 °C·min^{-1} (in nitrogen, with a 30 mL·min^{-1} airflow), to analyze the thermal stability and phase changes of the sample. An eight-channel isothermal calorimeter (I-CAL Flex, USA) was used to measure the hydration heat of each mixture at 20 °C for 3 d, and all raw materials were stored at 20 °C for at least 24 h before testing.

Table 3 Ratio of different biochar incorporated into cement composites

Samples	OPC (g)	Biochar (g)	W/C
Control (Ref)	400	0	0.4
A1, A2, A3	396	4	0.4
A1, A2, A3	392	8	0.4
A1, A2, A3	388	12	0.4
A1, A2, A3	380	20	0.4

A1, A2, and A3 are BC300-cement composites, BC500-cement composites, BC700-cement composites, respectively.

Data analysis and quantification of relevant emissions

The pseudo-first-order (Pfo), pseudo-second-order (Pso), and Avrami models were utilized to describe the adsorption kinetic profile of CO_2. Here are further explanations of these model equations[32]:

Pfo modeling:

$$q_t = q_e\left(1 - e^{-k_1 t}\right) \tag{1}$$

Pso modeling:

$$q_t = \frac{tk_2 q_e^2}{1 + q_e t k_2} \tag{2}$$

Avrami modeling:

$$q_t = q_e\left[1 - e^{-(k_A t)^n}\right] \tag{3}$$

where, q_t (mg·g^{-1}) and q_e (mg·g^{-1}) represent the CO_2 adsorption at time t (min) and equilibrium, respectively. Furthermore, k_1 (l·min^{-1}), k_2 (g·[mg·min]$^{-1}$), and k_A (l·min^{-1}) are adsorption rate constants.

The primary greenhouse gases (e.g., CO_2 and CH_4) were quantified in relation to biochar cement-related substances. The emissions in this study are quantified based on the mass of each component as listed in Table 3 (e.g., 4 g of biochar, 396 g of cement, and 160 g of water). Additionally, Supplementary Table S2 and S3 provides detailed quantification information.

Results and discussion

Previous studies have shown that the micropores of biochar provide a large SSA to accommodate adsorbates, while the mesopores promote rapid mass transfer, resulting in fast adsorption equilibrium[3]. Specifically, pores less than 0.8 nm are beneficial for the CO_2 uptake by biochar under atmospheric pressure. The BET results indicate that the SSA of alkali-modified biochar was reduced, and the microporous structure was improved, as listed in Table 4. This is attributed to the corrosive nature of alkali, which alters micropore volume and causes the collapse of mesopores and macropores, thereby affecting its SSA. This result provides a reference for understanding CO_2 adsorption by biochar in the following section.

In all samples, the alkali-modified biochar was primarily characterized by changes in peak intensities, while the functional group types do not change significantly (Fig. 2). It is observed that the vibrations of the non-conjugated C=O group (1,734 cm^{-1}), phenol (1,448 cm^{-1}), and aromatic hydrocarbons (1,190 cm^{-1}) were diminished after alkali modification in biochar prepared at low pyrolysis temperatures[33]. This is mainly attributed to alkali modification, which removes soluble components from the biochar through a corresponding chemical reaction. For example, phenol produces

Table 4 The surface area, cumulative adsorption pore volume, and adsorption average pore size of the different biochars

Sample	BET surface area ($m^2 \cdot g^{-1}$)	Adsorption average pore size (nm)	Cumulative adsorption pore volume ($cm^3 \cdot g^{-1}$)
BC300	9.804	7.158	0.019
SP300	18.528	6.425	0.022
BC500	36.913	5.974	0.024
SP500	54.658	6.362	0.040
BC700	140.013	4.676	0.044
SP700	150.064	4.487	0.047
MBC300	2.894	6.924	0.012
MSP300	17.194	4.688	0.017
MBC500	29.691	4.613	0.033
MSP500	36.060	4.683	0.026
MBC700	124.607	4.676	0.044
MSP700	134.141	4.057	0.034

highly soluble phenol salts in an alkaline environment, which are eventually removed. Therefore, the FTIR spectra of the modified biochar appeared smoother than those of the original biochar. Moreover, the stretching vibrational peak of hydroxyl groups (–OH) at 3,341 cm^{-1} and the vibrational peaks of ester bonds (C=C and C=O) at 1,568 cm^{-1} were enhanced due to the oxidative cleavage of unstable C–C bonds and the formation of C–O bonds[34]. It is noteworthy that the functional group types of biochar decrease with increasing pyrolysis temperature. Therefore, alkali modification does not affect high-temperature pyrolyzed biochar as significantly as it does low-temperature pyrolyzed biochar.

As shown in Fig. 3, bulges were consistently observed between 2θ = 12 and 25° in all samples, primarily resulting from the presence of amorphous carbon in the biochar, indicating that alkali modification has eroded its surface. Furthermore, the diffraction peaks at 20.8, 26.6, and 36.5° correspond to SiO_2, with the most prominent peak appearing at 2θ = 26.6°[35]. The results show that the SiO_2 diffraction peaks of the original biochar became more pronounced after alkali modification. However, alkali modification had a lesser effect on the SiO_2 peak of SP. This could be due to changes in the structure or composition of the SP obtained from the original biochar after physical separation in an ultrasonic machine, making it less susceptible to alkali modification. Moreover, the SiO_2 diffraction peaks of the biochar became more pronounced with increasing pyrolysis temperature, which resulted from the fact that the temperature affects the morphology of SiO_2, thereby influencing its volcanic ash effect in cement composites.

Figure 4 shows the Raman spectral results in the range of 1,000–2,000 cm^{-1} for different biochar. In all samples, two main bands were observed: the D band (1,340–1,350 cm^{-1}), and the G band (1,580–1,600 cm^{-1}). The D band corresponds to disordered structures resulting from defects in the aromatic ring system, such as layer misalignment, grain size, or edge state in the biochar. The G band represents the graphite strip and is caused by the breathing of aromatic rings[36]. It is reported that the degree of biochar graphitization is usually represented by the ratio of the D and G band peak intensities (I_D/I_G). As the I_D/I_G ratio decreases, the more ordered the carbon structure and the fewer defects in the biochar[37]. The results demonstrated a consistent upward trend in I_D/I_G with increasing

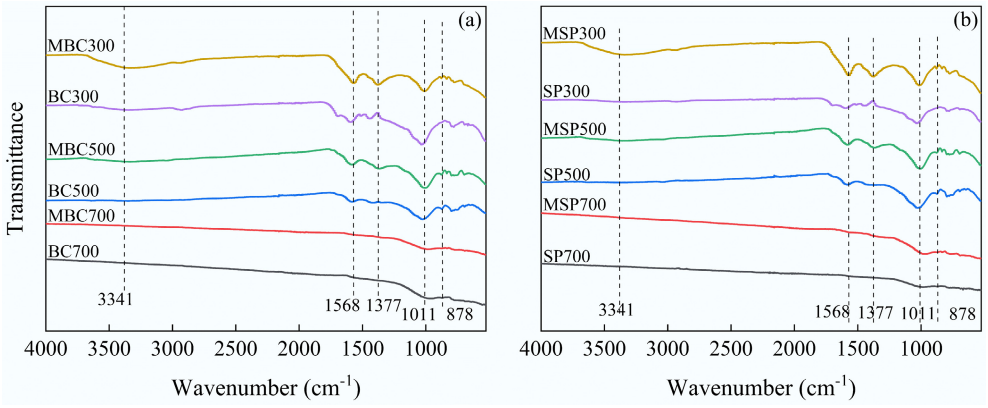

Fig. 2 Results of FTIR of (**a**) modified original biochar, and (**b**) modified SP.

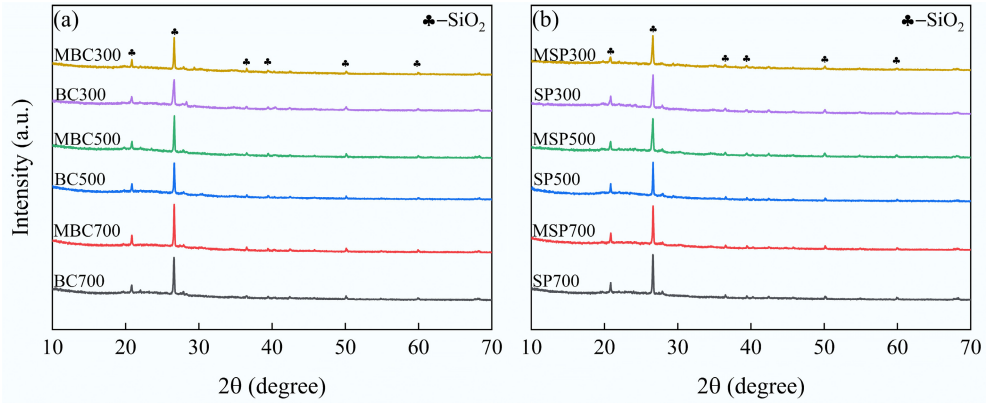

Fig. 3 Results of XRD of (**a**) modified original biochar, and (**b**) modified SP.

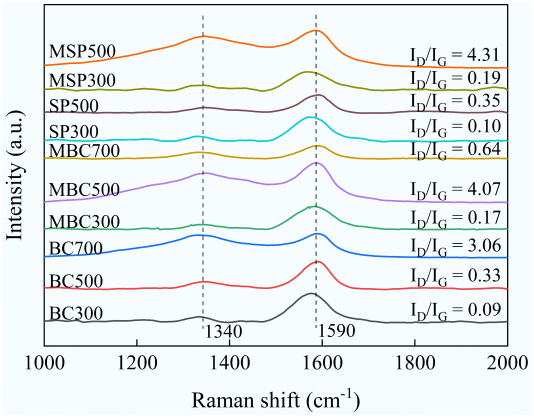

Fig. 4 Raman spectra characterization of different biochar samples.

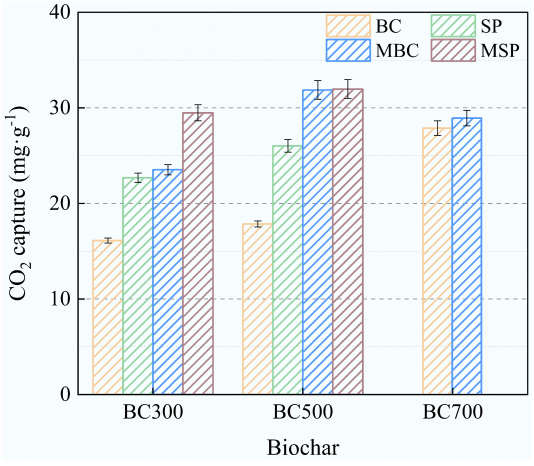

Fig. 5 CO_2 uptake by different biochar at room temperature.

biochar pyrolysis temperature, indicating an increase in defective aromatic ring structures. A slight increase in the I_D/I_G ratio was observed in SP relative to the original biochar, which may result from the disruption of the ordered carbon structure during ultrasonic separation. Furthermore, the I_D/I_G of the original biochar and SP at both 300 and 500 °C pyrolysis temperatures were smaller than those of their corresponding modified component. However, the opposite trend was observed for pyrolyzed biochar at 700 °C. This may be due to alkali modification disrupting the partially ordered carbon structure of the biochar pyrolyzed at 300 and 500 °C. However, the removal of impurities by alkali modification in biochar pyrolyzed at 700 °C may counteract this adverse effect.

Figure 5 shows the CO_2 adsorption by biochar at room temperature. The results indicate that the CO_2 uptake was higher by SP than by the original biochar. This could be due to the high ash content, which blocks the micropores in the original biochar and prevents surface alkaline active sites from effectively interacting with CO_2 molecules[38]. Interestingly, the modified biochar and SP in this study showed better CO_2 capture performance. This may be due to the enhancement of the microporous structure and pH of the biochar by alkali modification, which is consistent with the BET results. However, among all the modified biochar samples, MBC500 exhibited the highest CO_2 adsorption capacity. Combined with the Raman spectroscopy results this indicates that the microporous structure and alkalinity of the biochar are not all determinants of CO_2 adsorption, and that I_D/I_G is also one of the CO_2 adsorption factors.

The Pfo, Pso, and Avrami models were employed to describe the CO_2 adsorption process of different biochar (Fig. 6 and Table 5). It is reported that the Pfo model typically describes the reversible physical adsorption of CO_2 by biochar, whereas the Pso model is more suitable for representing chemical adsorption, which involves chemical bonding interactions between CO_2 and the biochar surface[39]. The Avrami model, a mathematical framework utilized to describe the kinetics of phase transitions, can also be applied to elucidate the processes of physical and chemical adsorption of CO_2 by biochar[40]. The results showed that all biochar samples reached over 70% of their maximum adsorption capacity within 10 min, indicating their rapid adsorption behavior. Furthermore, among all the kinetic models for CO_2 adsorption, the Avrami model yielded the highest R^2 values, indicating that the CO_2 adsorption in biochar is a result of both physical and chemical interactions. It is noteworthy that the R^2 values for the Pfo model are higher than those of the Pso model, indicating that CO_2 adsorption occurs primarily through physical interaction. In addition, the exponents n of the Avrami model are all higher than 1, indicating that CO_2 is adsorbed in different regions of the biochar with varying probabilities. This is because the adsorption process is non-homogeneous.

Figure 7 shows the exothermic rate during the hydration of cement composites incorporating 1% of different types of biochar. The first exothermic peak during the accelerated period appeared at 10 h, attributed to the hydration of tricalcium silicate (C_3S)[41]. The results show that the incorporation of biochar neither delays nor

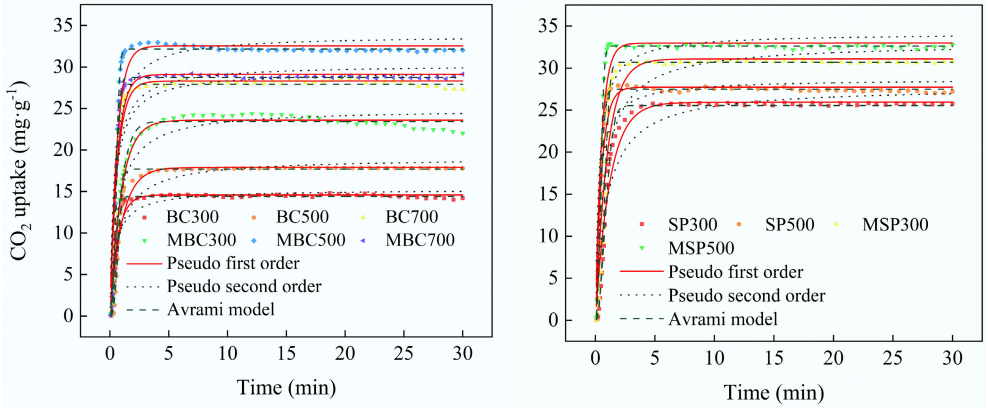

Fig. 6 Adsorption kinetic curves of different biochar samples at room temperature.

Table 5 Adsorption kinetics parameters of biochar to CO_2

Parameters	Model Pfo			Model Pso			Model Avrami			
	q_e	k_1	R^2	q_e	k_2	R^2	q_e	k_A	n	R^2
BC300	14.59	1.5087	0.9270	15.23	0.1489	0.8501	14.43	2.5684	2.2174	0.9974
BC500	17.99	0.9815	0.9265	19.03	0.0676	0.8825	17.69	1.6072	2.7757	0.9959
BC700	28.30	1.6080	0.9243	29.48	0.0829	0.8468	27.91	3.1152	2.2713	0.9951
MBC300	23.59	1.0378	0.9808	24.92	0.0613	0.9360	23.43	1.0987	1.2791	0.9886
MBC500	32.53	1.6775	0.9072	33.80	0.0770	0.8138	32.14	3.6354	2.5360	0.9982
MBC700	29.10	1.6533	0.9217	30.27	0.0838	0.8380	28.72	3.2764	2.3077	0.9981
SP300	25.93	0.8307	0.9509	27.70	0.0393	0.9057	25.53	0.9339	2.0888	0.9936
SP500	27.72	1.9289	0.9283	28.69	0.1096	0.8283	27.47	3.4575	2.0176	0.9960
MSP300	31.08	1.0106	0.9168	32.98	0.0416	0.8571	30.68	1.3309	2.7293	0.9978
MSP500	32.97	1.9945	0.9096	34.13	0.0949	0.8037	32.61	4.6009	2.3394	0.9989

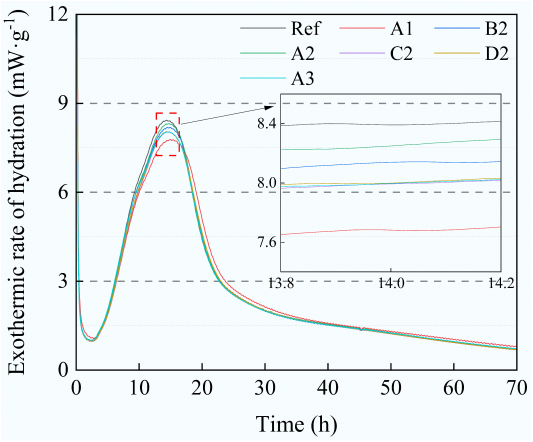

Fig. 7 Effect of different biochar additions on the exothermic rate of hydration of cement composites.

accelerates the hydration process. Furthermore, modified biochar with adsorbed CO_2 had lower heat escape here compared to the original biochar. This may be associated with CO_2-induced carbonation, as CO_2 adsorbed on modified biochar can convert some $Ca(OH)_2$ to carbonate. Related studies have reported that the calorific value of calcium carbonate solution (102 calories·g^{-1}) is lower than that of $Ca(OH)_2$ (557 calories·g^{-1})[42]. The degree of carbonation may influence the microstructural connectivity within the interfacial transition zone (ITZ) between the biochar and the cement matrix, resulting in different compressive strengths of samples with different CO_2 contents.

Figure 8 shows the compressive strength of different biochar cement composites. The results demonstrate that the 7-d compressive strength error bars were larger than those of the 28-d compressive strength. This may be because the test blocks are more fully hydrated and more stable in strength after 28 d. In all original biochar-cement composites, the compressive strength first increases and then decreases with the increase of the biochar pyrolysis temperature. Additionally, the compressive strength peaked at a 2% biochar dosage. This may be because different pyrolysis temperatures result in different nucleation, filling, and internal curing effects of biochar in cement composites, leading to different amounts of hydration products[43]. For example, BET results indicate that higher pyrolysis temperatures led to a higher SSA of biochar, contributing to hydration promotion. However, these effects cannot compensate for the reduction in cement content caused by the addition of biochar. Moreover, excessive biochar dosage increases porosity, which negatively affects the composites and makes them more prone to microcrack formation under pressure[44]. Interestingly, the compressive strength of SP at 7 d was lower than that of BC, while the opposite trend was observed at 28 d, which may be because the biochar volcanic ash effect has a more pronounced influence on the early compressive strength. In addition, CO_2 adsorption on biochar is a physically exothermic process, thus facilitating the CO_2 desorption process as the temperature increases. In this context, the heat generated from the cement hydration process may lead to the release of some CO_2 from the modified biochar, thereby affecting the compressive strength of the cement composites. For example, the moderate addition of modified biochar with adsorbed CO_2 promotes composites with higher compressive strengths compared to control and original biochar-cement

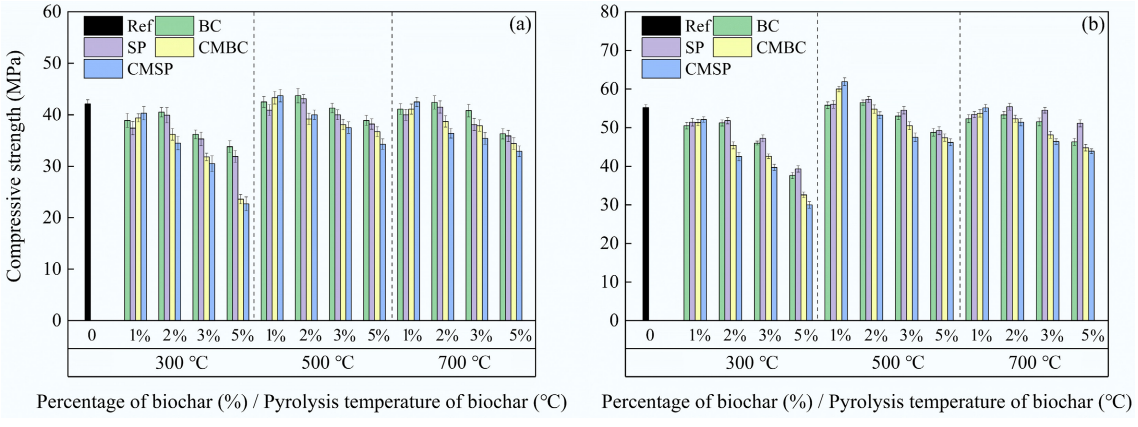

Fig. 8 Compressive strength results of different biochar cement composites tested at **(a)** 7, and **(b)** 28 d.

composites. This is mainly attributed to the presence of CO_2, which promotes internal carbonation of the cement composite, resulting in a denser structure. However, excessive CO_2 incorporation can lead to an excessive expansion carbonation reaction around the biochar, which may introduce more voids in the cement composite and affect the compressive strength development[45]. Moreover, the optimization of the physicochemical properties of the biochar material also contributes to the compressive strength of the cement composites, as shown by the BET, XRD, and FTIR results. Compared to other pyrolysis temperatures, biochar pyrolyzed at 300 °C exhibited a higher fluctuation in the compressive strength of composites with increasing doping, which may be associated with the formation of fatty acids at low temperatures. In conclusion, the beneficial internal curing effects and the negative impacts of modified biochar for CO_2 adsorption should be carefully balanced.

Figure 9a shows the XRD results of cement composites incorporating 1% biochar. Meanwhile, the most prominent peak (2θ = 18°) in the XRD spectrum was identified as semi-quantitative analysis of $Ca(OH)_2$, and its integral area was analyzed (Supplementary Fig. S1). The results indicate that the primary crystalline phases $Ca(OH)_2$, AFt, C_3S, Belite (C_2S), $CaCO_3$, and SiO_2 were present in all samples[41]. Therefore, the addition of biochar resulted in negligible changes to the crystalline phases. Moreover, the relatively high $Ca(OH)_2$ content of BC500 and SP500 at 2θ = 18° compared to the control may be attributed to the promotion of cement hydration by biochar. However, BC300 and BC700 exhibited the opposite results, which may be due to the difference in pyrolysis temperatures, resulting in differences in the characteristics of the biochar itself, thereby affecting the performance of cement composites. This echoes the results of the physicochemical property tests of biochar mentioned above, including XRD, FTIR, and BET. In addition, the lower $Ca(OH)_2$ content in modified biochar with adsorbed CO_2, along with the increased peak intensity of calcite at 2θ = 18° can be attributed to the exothermic process of cement hydration, resulting in the desorption of CO_2 from the biochar and the formation of $CaCO_3$ by combining CO_2 with some $Ca(OH)_2$[32].

The FTIR results of the cement composites after 28 d are shown in Fig. 9b. The results demonstrate that the functional groups in all samples had similar energies, indicating that the samples contained the same composition. It is noteworthy that typical functional groups of biochar may not be observed in the samples because the characteristic peak intensity of biochar from corn stover pyrolysis may overlap with the hydration products. For example, the peak at 1,563 cm^{-1} is attributed to aromatic C=C in biochar or C=O vibrations in hydration products[46]. This is consistent with the FTIR results for biochar. Additionally, the peaks at 1,413 and 873 cm^{-1} represent the bending vibration of CO_3^{2-}, and the peak at 950 cm^{-1} corresponds to the vibration of calcium silicate hydrate (C-S-H)[47]. In general, these peak strengths are considered to have some correlation with the strength of the cement composite. The peak intensities of BC300 and BC700 are slightly reduced at these locations and increased for the other biochar samples compared to the control. This demonstrates that, except for BC300 and BC700, the other 1% incorporation of biochar promoted the formation of more hydration products. This is consistent with the compressive strength results.

The SEM results of the cement composites cured for 28 d are shown in Fig. 10. Layered $Ca(OH)_2$ crystals and flocculent C-S-H gels were observed in all samples[46]. This indicates that the incorporation of biochar had no effect on the type of hydration products in cement composites. Adding an optimal amount of biochar to the cement composites promoted the formation of hydration products, resulting in a more compact internal structure than that of the control group. Previous works have demonstrated that, due to van der Waals forces, cracks and pores cause ITZ connections to be weak and prone to fracture[48]. In this study, large pores were observed in the ITZ between biochar particles pyrolyzed at 300 and 700 °C and the cement matrix. As a result, the compressive strength of the biochar-cement composites decreased. Furthermore, the composites with C2 and D2 exhibited a denser microstructure, correlating with their improved strength in this work.

The TG and DTG curves of the biochar-cement composites after 28 d of air curing are shown in Fig. 11. The results indicate that AFt, aluminate ferrite monosulfate (AFm), and C-S-H decomposed between 50–200 °C; $Ca(OH)_2$ decomposed between 420–540 °C; and $CaCO_3$ decomposed between 600–800 °C, exhibiting significant decomposition peaks[20]. It is noteworthy that when the test temperature exceeded the biochar pyrolysis temperature, there was a slight loss of biochar. However, this mass loss is not accounted for in this study due to its negligible magnitude. It is reported that $Ca(OH)_2$ is an important indicator of the degree of hydration[46]. As listed in Table 6, the relatively high $Ca(OH)_2$ content in the A2 and B2 samples indicates that biochar promotes cement hydration. Moreover, C2 and D2 exhibited a significantly higher mass loss compared to the control group in the temperature range of 600 to 800 °C. This phenomenon is attributed to the decomposition of calcite, and a similar trend is observed in the XRD results. These result demonstrates that CO_2 adsorbed by biochar can effectively accelerate carbonation and enhance the strength of composites.

Figure 12 shows the hydration process of cement composites incorporating different types of biochar. In cement systems, CO_2 typically undergoes a reaction process involving dissolution, ion diffu-

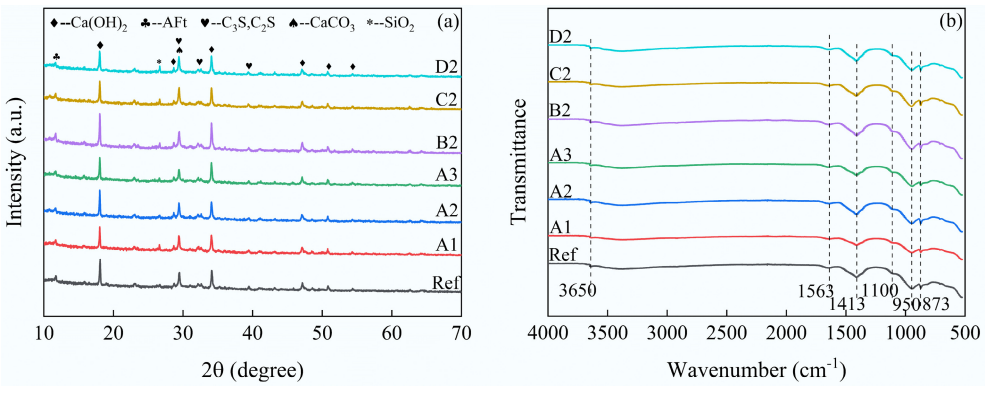

Fig. 9 Results of biochar-cement composites of **(a)** XRD, and **(b)** FTIR.

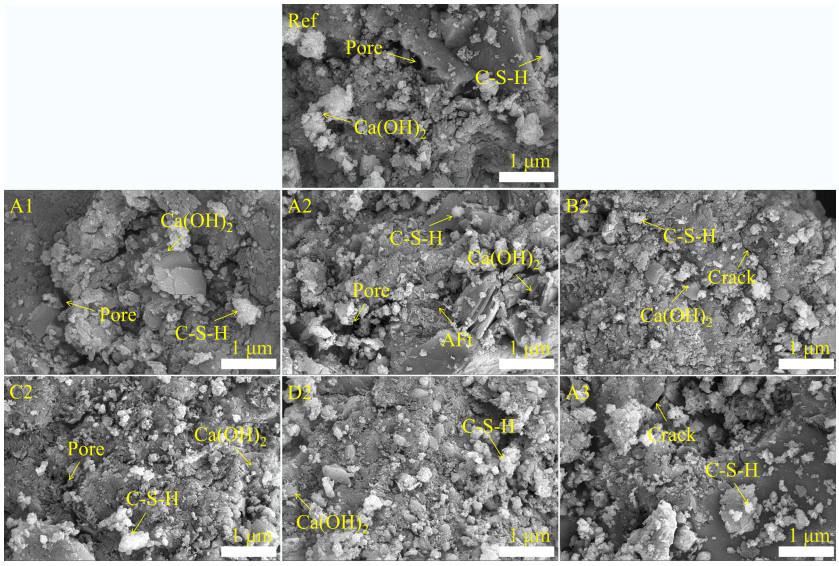

Fig. 10 SEM results for Ref, A1, A2, B2, C2, D2, A3.

Table 6 Mass loss of $Ca(OH)_2$ and $CaCO_3$ in various biochar cement composites (wt.%)

Item	$Ca(OH)_2$	$CaCO_3$
Ref	2.822	5.474
A1	2.685	5.989
A2	2.883	5.273
A3	2.806	6.164
B2	2.967	5.782
C2	2.759	6.451
D2	2.693	6.511

sion, and precipitation. CO_2 dissolves and ionizes in the presence of water, forming CO_3^{2-} and H^+. Notably, this process is exothermic and accompanied by some evaporation of the mixing water. Meanwhile, cement particles rapidly release Ca^{2+} upon dissolution. In the presence of water and high temperatures, Ca^{2+} reacts with CO_3^{2-} to form a supersaturated solution, which subsequently leads to the precipitation of $CaCO_3$[49]. The compressive strength results confirm this observation. In this period, the rapid formation of C-S-H contributed to the further enhancement of the corresponding strength. Moreover, the C-S-H formed around the biochar-saturated region undergoes decalcification and gradually transforms into SiO_2 gel, leading to a reduction in the pH of the pore solution[50].

The quantified emission values of biochar cement composites are shown in Table 7, Supplementary Tables S2, and S3. The results indicate that cement production is the principal source of carbon emissions in biochar-cement composites. However, the incorporation of biochar contributes to a reduction in CO_2 emissions. Moreover, the preparation of biochar avoids landfill disposal of biomass. Nevertheless, the carbon emissions caused by the use of chemical reagents may outweigh the environmental benefits gained from the process. It was observed that, regardless of the pyrolysis temperature of biochar, the carbon reduction achieved by applying SP in cement exceeded the emissions generated during the preparation of SP from BC. Furthermore, avoided emissions due to biochar production comprise two components: carbon sequestered within the biochar and replacing fossil fuels with syngas and bio-oil of equivalent caloric value. In short, the utilization of biochar reduces the environmental impacts associated with waste management.

Conclusions

This work introduces biochar as a carbon sequestration admixture for cement composites. The results indicate that increasing the pyrolysis temperature enhanced the CO_2 adsorption capacity of both the original biochar and SP, with SP exhibiting a greater capacity than the

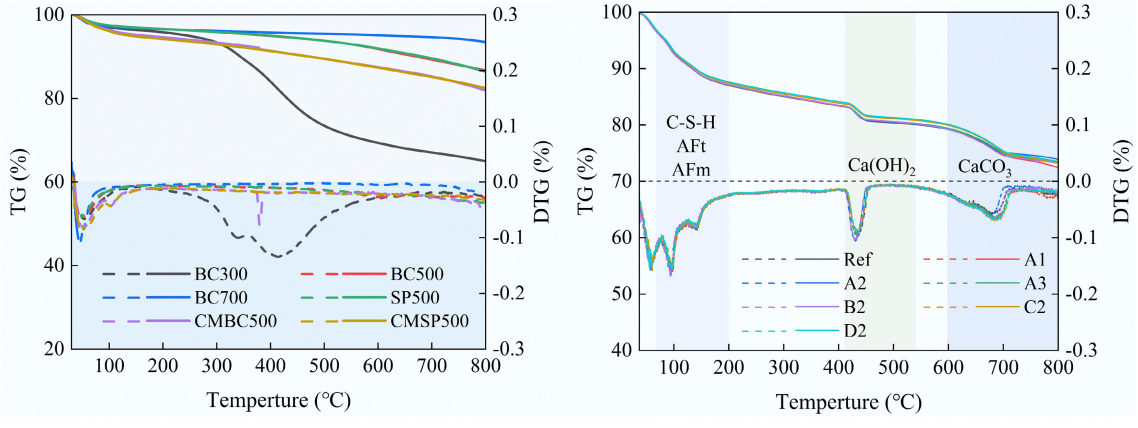

Fig. 11 Results of TG and DTG.

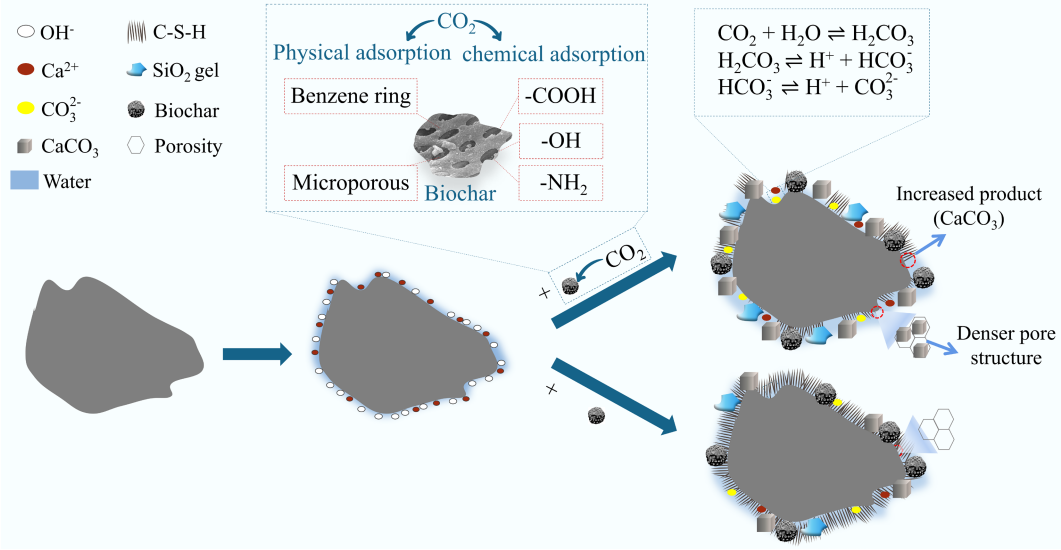

Fig. 12 Influence of different biochar on the cement hydration mechanism.

Table 7 Carbon emissions of biochar cement composites

Materials/processes (10^{-5} kg)	Without BC	A2/B2/C2/D2 (1%)	A2/B2/C2/D2 (2%)	A2/B2/C2/D2 (3%)	A2/B2/C2/D2 (5%)	Ecoinvent inputs
OPC	29400	29100	28800	28500	27900	Cement production, Portland
Water	2.69	2.69/4.93/4.37/6.61	2.69/7.17/6.05/10.53	2.69/9.41/7.73/14.45	2.69/13.89/11.09/22.29	Tap water production, conventional treatment
BC500 production (–)	–	138.33/173.94/ 138.33/173.94	276.66/347.88/ 276.66/347.88	414.99/521.82/ 414.99/521.82	691.65/869.70/ 691.65/869.70	Biochar preparation
NaOH	–	0/0/636/636	0/0/1272/1272	0/0/1908/1908	0/0/3180/3180	China carbon emissions database
Transportation	164.4	168.48/168.62/ 168.48/168.62	172.55/172.84/ 172.55/172.84	176.63/177.07/ 176.63/177.07	184.77/185.52/ 184.77/185.52	Transportation distance: 30 km
Avoided emission (–)	–	0.59/0.60/0.59/0.60	1.17/1.20/1.17/1.20	1.76/1.81/1.76/1.81	2.93/3.01/2.93/3.01	–
Net emission	29567.088	29132.25/29099.01/ 29769.93/29736.69	28697.41/28630.93/ 29972.77/29906.29	28262.57/28162.85/ 30175.61/30075.89	27392.88/27226.70/ 30581.28/30415.10	–

original biochar. Alkali modification enhanced the microporous structure of biochar, thereby further increasing its CO_2 capture capacity. Notably, the adsorption process was predominantly governed by physical adsorption, with chemical adsorption playing a secondary role. In addition, an appropriate dosage of biochar can mitigate the adverse effects associated with reduced cement content through the micro-filler effect, volcanic ash effect, and secondary hydration effect. In contrast, SP promoted the strength of cement composites better than the original biochar. However, excessive biochar addition resulted in a reduction in strength due to the increased porosity. Additionally, incorporating an appropriate amount of CO_2-saturated modified biochar accelerated the carbonization process, resulting in the formation of a denser microstructure. However, excessive CO_2 triggered an overreaction in the carbonation process of biochar-cement composites, resulting in the formation of additional voids and a reduction in their mechanical properties. Additionally, the incorporation of biochar contributed to reducing the carbon footprint of cement composites. Future studies should further investigate the applicability of different modified biochar saturated with CO_2 at higher dosages. Additionally, comprehensive long-term durability evaluations, including resistance to environmental exposures, such as sulfate attack and chloride penetration, are crucial for fully assessing the practical applicability and benefits of biochar cement composites.

Supplementary information

It accompanies this paper at: https://doi.org/10.48130/bchax-0025-0004.

Author contributions

All authors contributed to the study conception and design. Data curation, validation, and formal analysis were performed by Binglin Guo, Ping Ye, Huyong Qin, Cheng Wang, Yang Liu, Yuyang Chen, Pengfei Bian, Di Lu, Lei Wang, Tongsheng Zhang, and Weiping Zhao. Project administration and funding acquisition were performed by Binglin Guo. Investigation and supervision were performed by Binglin Guo, Lei Wang, Tongsheng Zhang, Binggen Zhan, and Qijun Yu. Conceptualization was performed by Binglin Guo, Lei Wang, and Tongsheng Zhang. Review and editing were performed by Binglin Guo, Lei Wang, and Tongsheng Zhang. Methodology was performed by Binglin Guo and Ping Ye. The original draft was produced by Ping Ye. All authors commented on previous versions of the manuscript and approved the final version of the manuscript.

Data availability

The datasets used or analyzed during the current study are available from the corresponding author upon reasonable request.

Funding

This work was provided to BG by 'the Fundamental Research Funds for the Central Universities' (Grant No. PA20255GDGP0027), and 'the University Synergy Innovation Program of Anhui Province' (Grant No. GXXT–2023–104).

Declarations

Competing interests

The authors declare that they have no conflict of interest.

Author details

[1]College of Civil Engineering, Hefei University of Technology, Hefei, Anhui 230009, China; [2]Engineering Research Center of Low-carbon Technology and Equipment for Cement-based Materials, Ministry of Education, Hefei University of Technology, Hefei, Anhui 230009, China; [3]Anhui Research Center of Low-carbon Technology for Cement-based Materials, Hefei University of Technology, Hefei, Anhui 230009, China; [4]State Key Laboratory of Clean Energy Utilization, Zhejiang University, Hangzhou, Zhejiang 310027, China; [5]School of Materials Science and Engineering, South China University of Technology, Guangzhou, Guangdong 510640, China

References

[1] Wang Q, Luo J, Zhong Z, Borgna A. 2011. CO_2 capture by solid adsorbents and their applications: current status and new trends. *Energy & Environmental Science* 4(1):42–55

[2] Wang L, Chen L, Poon CS, Wang CH, Ok YS, et al. 2021. Roles of biochar and CO_2 curing in sustainable magnesia cement-based composites. *ACS Sustainable Chemistry & Engineering* 9(25):8603–8610

[3] Xu S, Chen J, Peng H, Leng S, Li H, et al. 2021. Effect of biomass type and pyrolysis temperature on nitrogen in biochar, and the comparison with hydrochar. *Fuel* 291:120128

[4] Chen L, Zhang Y, Wang L, Ruan S, Chen J, et al. 2022. Biochar-augmented carbon-negative concrete. *Chemical Engineering Journal* 431:133946

[5] Munir MT, Ul Saqib N, Li B, Naqvi M. 2023. Food waste hydrochar: an alternate clean fuel for steel industry. *Fuel* 346:128395

[6] Wang Q, Xue M, Lin BL, Lei Z, Zhang Z. 2020. Well-to-wheel analysis of energy consumption, greenhouse gas and air pollutants emissions of hydrogen fuel cell vehicle in China. *Journal of Cleaner Production* 275:123061

[7] Afari DB, Coker J, Narku-Tetteh J, Idem R. 2018. Comparative kinetic studies of solid absorber catalyst (K/MgO) and solid desorber catalyst (HZSM-5)-aided CO_2 absorption and desorption from aqueous solutions of MEA and blended solutions of BEA-AMP and MEA-MDEA. *Industrial & Engineering Chemistry Research* 57(46):15824–15839

[8] Chen L, Zhang Y, Labianca C, Wang L, Ruan S, et al. 2022. Carbon-negative cement-bonded biochar particleboards. *Biochar* 4(1):58

[9] Zhang Y, Wang S, Feng D, Gao J, Dong L, et al. 2022. Functional biochar synergistic solid/liquid-phase CO_2 capture: a review. *Energy & Fuels* 36(6):2945–2970

[10] Manyà JJ. 2012. Pyrolysis for biochar purposes: a review to establish current knowledge gaps and research needs. *Environmental science & technology* 46(15):7939–7954

[11] Li B, Li M, Xie X, Li C, Liu D. 2024. Pyrolysis of rice husk in molten lithium chloride: Biochar structure evolution and CO_2 adsorption. *Journal of the Energy Institute* 113:101526

[12] Lahijani P, Mohammadi M, Mohamed AR. 2018. Metal incorporated biochar as a potential adsorbent for high capacity CO_2 capture at ambient condition. *Journal of CO_2 utilization* 26:281–293

[13] Ghanbari S, Kamath G. 2019. Dynamic simulation and mass transfer study of carbon dioxide capture using biochar and MgO-impregnated activated carbon in a swing adsorption process. *Energy & fuels* 33(6):5452–5463

[14] Zhu Y, Li H, Zhang G, Meng F, Li L, et al. 2018. Removal of hexavalent chromium from aqueous solution by different surface-modified biochars: Acid washing, nanoscale zero-valent iron and ferric iron loading. *Bioresource technology* 261:142–150

[15] Ding S., Liu Y. 2020. Adsorption of CO_2 from flue gas by novel seaweed-based KOH-activated porous biochars. *Fuel* 260:116382

[16] Zhang Y, He M, Wang L, Yan J, Ma B, et al. 2022. Biochar as construction materials for achieving carbon neutrality. *Biochar* 4(1):59

[17] Asadi Zeidabadi Z, Bakhtiari S, Abbaslou H, Ghanizadeh AR. 2018. Synthesis, characterization and evaluation of biochar from agricultural waste biomass for use in building materials. *Construction and Building Materials* 181:301–308

[18] Gupta S, Kua HW, Low CY. 2018. Use of biochar as carbon sequestering additive in cement mortar. *Cement and Concrete Composites* 87:110–129

[19] Haris Javed M, Ali Sikandar M, Ahmad W, Tariq Bashir M, Alrowais R, et al. 2022. Effect of various biochars on physical, mechanical, and microstructural characteristics of cement pastes and mortars. *Journal of Building Engineering* 57:104850

[20] Choi WC, Yun HD, Lee JY. 2012. Mechanical properties of mortar containing bio-char from pyrolysis. *Journal of the Korea institute for structural maintenance and inspection* 16(3):67–74

[21] Xu F, Wei C, Zeng Q, Li X, Alvarez PJJ, et al. 2017. Aggregation behavior of dissolved black carbon: implications for vertical mass flux and fractionation in aquatic systems. *Environmental science & technology* 51(23):13723–13732

[22] Giannetta B, Plaza C, Galluzzi G, Benavente-Ferraces I, García-Gil JC, et al. 2024. Distribution of soil organic carbon between particulate and mineral-associated fractions as affected by biochar and its co-application with other amendments. *Agriculture. Ecosystems & Environment* 360:108777

[23] Yue L, Lian F, Han Y, Bao Q, Wang Z, et al. 2019. The effect of biochar nanoparticles on rice plant growth and the uptake of heavy metals: Implications for agronomic benefits and potential risk. *Science of The Total Environment* 656:9–18

[24] Smebye A, Alling V, Vogt RD, Gadmar TC, Mulder J, et al. 2016. Biochar amendment to soil changes dissolved organic matter content and composition. *Chemosphere* 142:100–105

[25] Zhang K, Mao J, Chen B. 2019. Reconsideration of heterostructures of biochars: morphology, particle size, elemental composition, reactivity and toxicity. *Environmental Pollution* 254:113017

[26] Ye P, Guo B, Qin H, Wang C, Liu Y, et al. 2025. Investigation of the effects of the biochar in different fractions on cement composites. *Cement and Concrete Composites* 162:106142

[27] Kim JH, Lee DH, Mendoza JA, Lee MY. 2024. Applying machine learning random forest (RF) method in predicting the cement products with a co-processing of input materials: optimizing the hyperparameters. *Environmental Research* 248:118300

[28] Shafeeyan MS, Daud WMAW, Houshmand A, Arami-Niya A. 2011. Ammonia modification of activated carbon to enhance carbon dioxide adsorption: effect of pre-oxidation. *Applied Surface Science* 257(9):3936–3942

[29] Ghani WAWAK, Mohd A, da Silva G, Bachmann RT, Taufiq-Yap YH, et al. 2013. Biochar production from waste rubber-wood-sawdust and its potential use in C sequestration: chemical and physical characterization. *Industrial Crops and Products* 44:18–24

[30] Creamer AE, Gao B, Zhang M. 2014. Carbon dioxide capture using biochar produced from sugarcane bagasse and hickory wood. *Chemical Engineering Journal* 249:174–179

[31] GB/T 17671-2021. 2021. Test Method of Cement Mortar Strength, Ministry of Housing and Urban-Rural Development of the People's Republic of China, Beijing, China

[32] Cao W, Xu H, Zhang X, Xiang W, Qi G, et al. 2023. Novel post-treatment of ultrasound assisting with acid washing enhance lignin-based biochar for CO_2 capture: adsorption performance and mechanism. *Chemical Engineering Journal* 471:144523

[33] Pińkowska H, Wolak P, Złocińska A. 2012. Hydrothermal decomposition of alkali lignin in sub-and supercritical water. *Chemical Engineering Journal* 187:410–414

[34] Pradhan D, Singh RK, Bendu H, Mund R. 2016. Pyrolysis of Mahua seed (Madhuca indica)–production of biofuel and its characterization. *Energy Conversion and Management* 108:529–538
[35] Qian L, Chen B. 2013. Dual role of biochars as adsorbents for aluminum: the effects of oxygen-containing organic components and the scattering of silicate particles. *Environmental Science & Technology* 47(15):8759–8768
[36] Zhang C, Shao Y, Zhang L, Zhang S, Westerhof RJM, et al. 2020. Impacts of temperature on evolution of char structure during pyrolysis of lignin. *Science of the total environment* 699:134381
[37] Dissanayake PD, Choi SW, Igalavithana AD, Yang X, Tsang DCW, et al. 2020. Sustainable gasification biochar as a high efficiency adsorbent for CO_2 capture: A facile method to designer biochar fabrication. *Renewable and Sustainable Energy Reviews* 124:109785
[38] Solís RR, del Carmen González M, Blázquez G, Calero M, Martín-Lara MÁ. 2023. Activated char from the co-pyrolysis of polystyrene and olive stone mixtures for the adsorption of CO_2. *Journal of Environmental Chemical Engineering* 11(6):111370
[39] Raganati F, Alfe M, Gargiulo V, Chirone R, Ammendola P. 2019. Kinetic study and breakthrough analysis of the hybrid physical/chemical CO_2 adsorption/desorption behavior of a magnetite-based sorbent. *Chemical Engineering Journal* 372:526–535
[40] Choi J, Nam H, Carter S, Capareda SC. 2017. Tuning the physicochemical properties of biochar derived from Ashe juniper by vacuum pressure and temperature. *Journal of environmental chemical engineering* 5(4):3649–3655
[41] Wang L, Chen L, Tsang DCW, Guo B, Yang J, et al. 2020. Biochar as green additives in cement-based composites with carbon dioxide curing. *Journal of Cleaner Production* 258:120678
[42] Carlson MW, Forbrich LR. 1938. Correlation of methods for measuring heat of hydration of cement. *Industrial & Engineering Chemistry Analytical Edition* 10(7):382–386
[43] Gupta S, Kua HW, Koh HJ. 2018. Application of biochar from food and wood waste as green admixture for cement mortar. *Science of the Total Environment* 619–620:419–435
[44] Odimegwu TC, Zakaria I, Abood MM, Nketsiah CBK, Ahmad M. 2018. Review on different beneficial ways of applying alum sludge in a sustainable disposal manner. *Civil Engineering Journal* 4(9):2230–2241
[45] Johannesson B, Utgenannt P. 2001. Microstructural changes caused by carbonation of cement mortar. *Cement and Concrete Research* 31(6):925–931
[46] Chen X, Li J, Xue Q, Huang X, Liu L, et al. 2020. Sludge biochar as a green additive in cement-based composites: Mechanical properties and hydration kinetics. *Construction and Building Materials* 262:120723
[47] Kakali G, Tsivilis S, Aggeli E, Bati M. 2000. Hydration products of C_3A, C_3S and Portland cement in the presence of $CaCO_3$. *Cement and Concrete Research* 30(7):1073–1077
[48] Tan K, Pang X, Qin Y, Wang J. 2020. Properties of cement mortar containing pulverized biochar pyrolyzed at different temperatures. *Construction and Building Materials* 263:120616
[49] Ye P, Guo B, Qin H, Wang C, Li J, et al. 2024. Investigation of the properties and sustainability of modified biochar-doped cement-based composite. *Cement and Concrete Composites* 153:105684
[50] Liu P, Zhang M, Mo L, Zhong J, Xu M, et al. 2022. Probe into carbonation mechanism of steel slag via FIB-TEM: The roles of various mineral phases. *Cement and Concrete Research* 162:106991

Copyright: © 2025 by the author(s). Published by Maximum Academic Press, Fayetteville, GA. This article is an open access article distributed under Creative Commons Attribution License (CC BY 4.0), visit https://creativecommons.org/licenses/by/4.0/.